DFT-Based Exploration of Transition Metal Phosphides for CO Reduction Reaction

Muhammad Awais * and Younes Abghoui *

Posted Date: 16 March 2026

doi: 10.20944/preprints202603.1119.v1

Keywords: carbon reduction; DFT; renewable energy resources; methane; formaldehyde; methanol; chemical physics

 doi:10.20944/preprints202603.1119.v1

Article

DFT-Based Exploration of Transition Metal Phosphides for CO Reduction Reaction

Muhammad Awais * and Younes Abghoui *

Science Institute of the University of Iceland, 102 Reykjavik, Iceland

* Correspondence: mua8@hi.is (M.A.); younes@hi.is (Y.A.)

Abstract

Ecosystem disruption is a significant challenge of the contemporary age, arising from substantial CO_2/CO emissions resulting from dependence on fossil fuels as a primary energy source. Scholars across several fields are striving to mitigate these severe greenhouse gas emissions. The most promising method is absorbing carbon and transforming it into sustainable energy. We sought to diminish CO levels by electrocatalytic reduction using innovative catalytic surfaces, namely transition metal phosphides (TMPs). During this work, VP is recognized as a very effective surface for CO reduction and the synthesis of methane, methanol, and formaldehyde at -0.68 V. Further, hydrogen evolution does not pose a challenge for any surface, despite all TMPs facilitating CO reduction. Overall, predictions from these DFT-guided predictions, experimentalists can get insight for their experimental validation and synthesize of active catalysts for CO conversion and green energy production.

Keywords: carbon reduction; DFT; renewable energy resources; methane; formaldehyde; methanol; chemical physics

1. Introduction

Following the Industrial Revolution, the first signs of an increase in carbon dioxide (CO_2) levels were discovered. This rise in CO_2 levels led to a significant deterioration of the climate, which was mostly caused by the overuse of fossil fuels. As a result, the transformation of carbon dioxide into a green fuel by electrochemical conversion is now a major topic of discussion among scientists and has garnered a great deal of interest [1–5]. Carbon dioxide reduction reaction (CO_2RR) is an efficient technique for the carbon-free synthesis of alcohol and hydrocarbon fuels. This method reduces CO_2 emissions and fosters the sustainable production of renewable fuels efficiently. CO_2RR may be conducted by four unique approaches: biochemical, photochemical, electrochemical, and thermochemical. Nevertheless, due to its configurable selectivity and reliable catalytic efficiency, electrochemical CO_2 reduction ranks among the most effective methods, since this process is exclusively reliant on electrode performance [6–14].

Historically, electrochemical CO_2RR have used specific metal-based catalysts, with copper being one of the most studied examples. Although copper is an exceptional catalyst for converting CO_2 into multiple products, it suffers from poor product selectivity. In a recent study, copper was shown to catalyze more than ten products at potentials exceeding -1.0 V, signifying its lack of selectivity and the challenge of product separation [15]. Similarly, another investigation identified copper as an electrode material characterized by both inadequate selectivity and a high overpotential requirement for CO_2RR [16]. Ultimately, improving activity and selectivity and the tailored design of catalysts are fundamental concerns of the present day. Consequently, researchers are focused on engineering new surfaces and more reliable reaction pathways to develop superior catalysts.

During CO_2RR, carbon monoxide and formic acid are the principal products that are observed during the initial phase of reduction, resulting from the first electron-proton transfer. However, further transition of electron-proton can lead to the formation of hydrocarbons and oxygenates, but this progression often results in a decline of selectivity and proficiency of CO_2RR [17–27]. To overcome

 doi:10.20944/preprints202603.1119.v1

this challenge, an improved strategy involves utilizing the carbon monoxide (first intermediate of CO_2RR) for direct electrocatalytic CO reduction (CORR). For instance, MoS_2 with the doping of transition metal atoms has been investigated for CORR, and chromium-doped MoS_2 having sulphur vacancies was reported as a promising surface to reduce the CO at -0.33V [28]. Similarly, metal-nitride phosphorene (MN_3@P) as a single-atom catalyst (SAC) has also been explored for CO reduction [29].

In this manuscript, we have done a comprehensive examination of TMPs as a catalytic surface for electrocatalytic reduction of CO under room conditions. The structures of TMPs under the current investigation are taken in the rocksalt crystalline orientation in (100) facets of 1:1 ratio of metal and phosphorus atoms. The theoretical framework based on density functional theory (DFT) is utilized here to assess their catalytic activity. Moreover, these surfaces can show excellent catalytic activities due to their adjustable structures, surprising conductivity and stability under the electrochemical environment [30,31]. It has already been reported that a decrease in thermal dissolution and improvement in stability of transition metal-based catalysts could be achieved through the introduction of phosphorous atoms [32]. Owing to their superior stability, effective activity, and economic pricing, these materials provide an appealing option for consideration as catalysts [33]. That is the main motive behind the selection of these surfaces in our analysis, and herein their catalytic activity is indicated by free energy diagrams based on their Gibbs free energy values.

2. Computational Research Details

In our present investigation, the Vienna ab initio Simulation Package (VASP) software has been used to examine TMPs as catalytic surfaces for CO reduction under ambient circumstances [34]. The electronic structural analysis was conducted using density functional theory (DFT), with the Revised Perdew-Burke-Ernzerhof (RPBE) as the exchange-correlation functional [35]. The computational precision and capabilities of RPBE for the development of certain properties, such as surface analysis and catalytic activity, which are crucial to the present inquiry, prompted its selection. Furthermore, the concordance between experimental findings and computational analyses conducted using RPBE was a primary reason for its selection in our current work [13,36–38]. For the optimization, a cut-off energy of 400 eV and a 4×4×1 Monkhorst-Pack K-point grid were used [39]. Secondly, we modified the essential conditions to achieve a relaxed structure with different adsorbates till their atomic forces went below 0.03 eV/Å. TMPs-based electrodes for catalyst design have 40 atoms and five layers, with a 1:1 ratio between the atoms of metal and phosphide, meaning that there are 20 atoms of metal and 20 phosphide atoms. During the investigation, the lower dual layers were restricted, but the remaining three layers were permitted to fully engage with reactants and participate entirely in chemical reactions. To illustrate this, we constructed Figure 1, whereby the borders of the TMPs in the x and y axes are treated as periodic, but a vacuum of 20 Å is implemented along the z-axis to mitigate the self-interaction of adjacent unit cells.

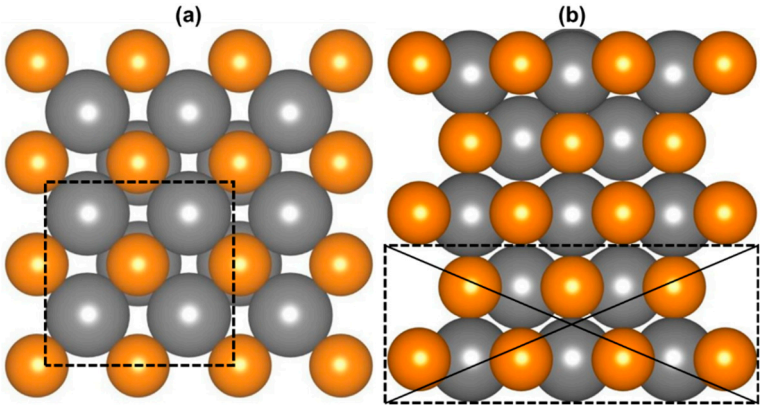

Figure 1. Side and top views of TMPs. Gray spheres indicate metal atoms, and orange represents phosphorous atoms. (a) Side view of TMP, where dotted lines indicate that the bottom two layers were considered fixed. (b) Top view of TMP, where dotted lines outline the unit cell, which is repeated along the x and y axes.

 doi:10.20944/preprints202603.1119.v1

The reaction pathways identified during the CO reduction into distinctive renewable products on TMPs were investigated using the thermochemical model (TCM), and the effect of applied potential was analyzed using the computational hydrogen electrode (CHE) [40–47]. To compute the adsorption energy (ΔE_{ads}), we used the following equation [48]:

$$\Delta E_{ads} = E_{Total\ system} - E_{System\ without\ adsorbate} - E_{adsorbed\ species} \quad (1)$$

To calculate the Gibbs free energy [49], we can use Eq. 2

$$\Delta G = \Delta E_{DFT} + \Delta E_{ZPE} - T\Delta S + \Delta G_{pH} + \Delta G_U \quad (2)$$

Here

ΔE_{DFT} = Energy difference between two intermediate states,

ΔE_{ZPE} = Zero-point energy correction,

$T\Delta S$ = Change in entropy,

Notably, ΔG_{pH} indicates the pH shift; the entire value of this component is 2.303 k_bTpH. K_b indicates the Boltzmann constant, T is temperature, and pH represents electrolytic pH; this is independent to overpotential; hence pH is 0 here. That is, ΔG_{pH} = zero. From Eq. 2, we have

$$\Delta G = \Delta E_{DFT} + \Delta E_{ZPE} - T\Delta S + (0) + \Delta G_U$$

$$\Delta G = \Delta E_{DFT} + \Delta E_{ZPE} - T\Delta S + \Delta G_U \quad (3)$$

ΔG_U = -neU, wherein n represents the number of electrons, e signifies the charge of an electron, and U symbolizes the applied potential [50–52]. In the absence of an applied potential, this term would equal 0, and Eq. 3 might be represented as such.

$$\Delta G = \Delta E_{DFT} + \Delta E_{ZPE} - T\Delta S \quad (4)$$

To get the value of the onset potential (OP) that occurs between the two steps with the maximum energy, the following equation [51] is utilized:

$$OP = -\Delta G_{max}/e \quad (5)$$

Where ΔG_{max} reflects the greatest variation in free energy seen between two steps that are next to each other in the reaction rout.

3. Results and Discussion

3.1. Surface Analysis

The surface analysis was the next phase in the forward examination, which came after we had obtained the optimal relaxed structures, which was the first step in our screening process. During this process, we looked at the slab's capacity to absorb a variety of different species. For example, the electrocatalytic reduction of carbon monoxide is the primary emphasis of our study. As a result, we studied the potential TMPs for carbon monoxide adsorption. Because of this, in addition to verifying the CO adsorption, we also examined the proton coverage at the various sites. The free energies of different adsorbed adsorbates have been summarized in Figure 2.

Figure 2 illustrates that the adsorption of CO is exergonic for HfP, TaP, TiP, VP, and ZrP; conversely, CrP and NbP exhibit unfavorable adsorption characteristics owing to the high energy demand for this process. Conversely, we examined the potential for water poisoning at each site by adsorbing water molecules to assess surface reactivity for this particular adsorption, then comparing the binding energies with CO adsorption. Figure 2 clearly demonstrates that water adsorption is consistently more endergonic than CO adsorption across all surfaces. Consequently, CO molecules are expected to occupy the catalyst surface prior to water, hence reducing the likelihood of water-induced surface poisoning. This indicates that all catalysts remain readily available and effective for CORR. In conclusion, only five TMPs (Hf, Ta, Ti, V, and Zr) exhibit high CO adsorption; thus, we will focus only on these surfaces for further investigation, since they are suitable for CORR with no risk of HER due to endergonic adsorption of proton on the surface when compared with CO adsorption.

 doi:10.20944/preprints202603.1119.v1

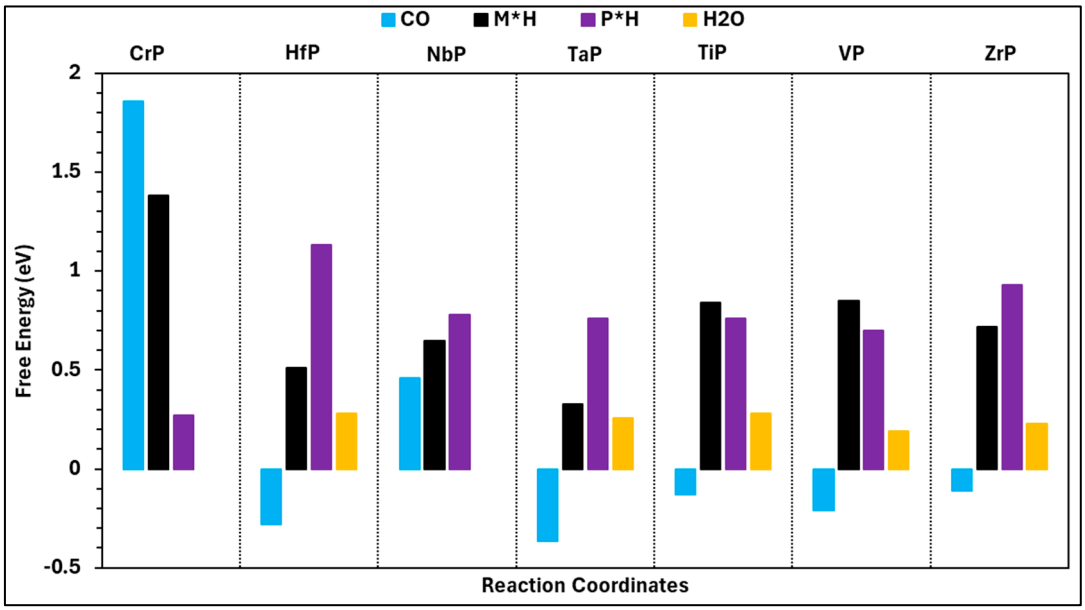

Figure 2. Gibbs free energy values of numerous species on TMPs.

3.2. Catalytic Activity Toward CO Reduction

CO reduction and conversion could lead to the production of methane, methanol and formaldehyde. These syntheses were observed after eight, six, and four electron proton transfers during electrocatalytic CORR. Additionally, we noticed that these formations were helped by different reaction routes, so we looked at the TMPs as catalyst surfaces and examined each route for the specific item. However, after thorough analysis, we only included the most promising free energy landscapes.

Our analysis demonstrated that VP has the highest activity among the several TMPs, since it generates formaldehyde at 0.69 eV, as seen in Figure 3. Additionally, the production of both methane and methanol was detected at the adjustable energy of 0.69 eV. Secondly, PDS during this reaction pathway was observed after the second protonation from CO*+PH* to CO*+PH*+MH*.

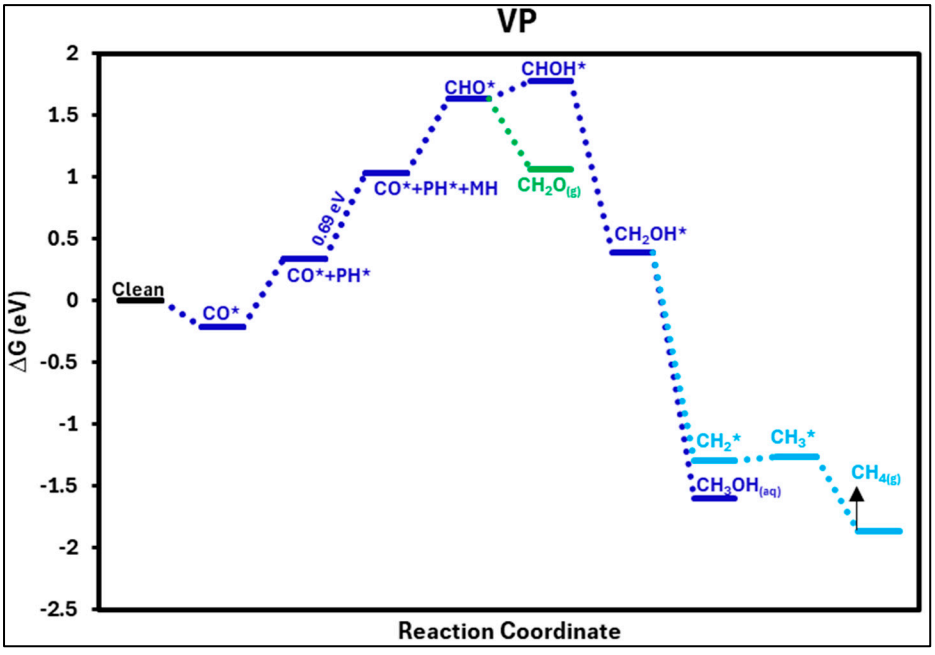

Figure 3. Free energy profile for CORR on the VP surface, exhibiting the catalytic activity for methane, methanol and formaldehyde production.

 doi:10.20944/preprints202603.1119.v1

HfP was also identified as a suitable substrate for the electrocatalytic synthesis of both methane and methanol. As seen in Figure 4, the whole reaction pathway progresses seamlessly, exhibiting the minimal energy requirenment of around 0.82 eV for CH_3OH and CH_4. This low energy clearly identifies HfP's catalytic effectiveness in facilitating the multi-electron CO reduction reaction. PDS arises at the second proton-electron transfer, especially during the transition from CO*+MH* to CO*+MH*+MH*

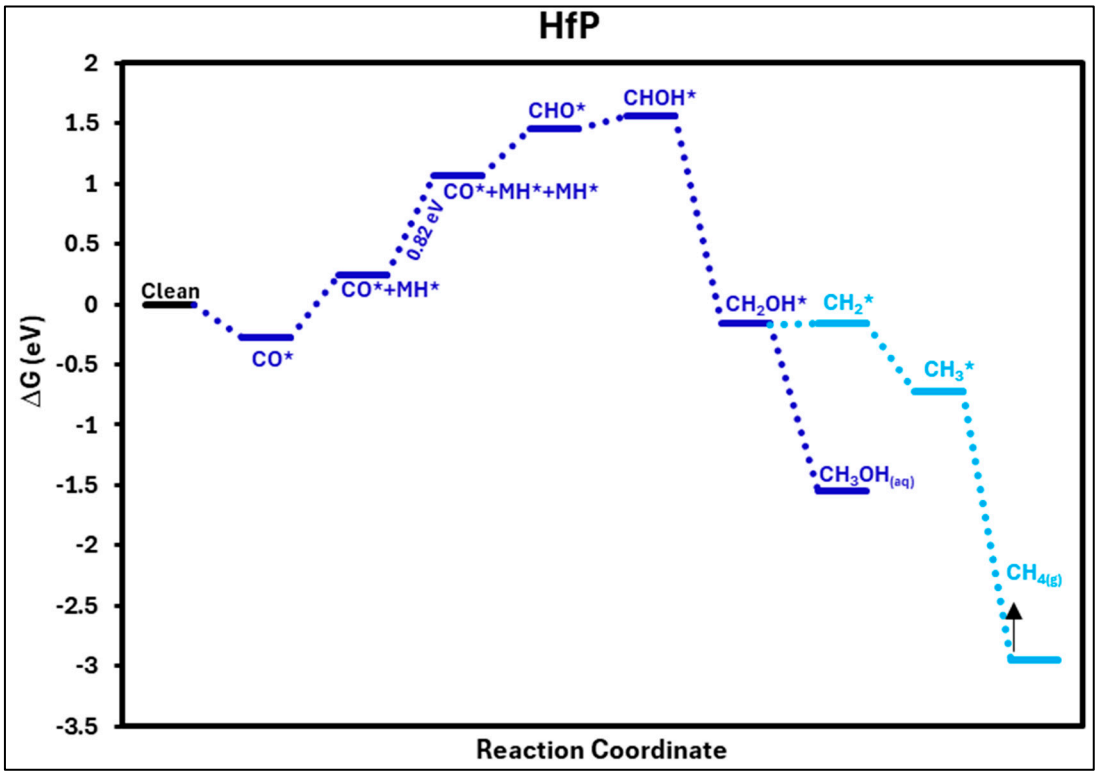

Figure 4. Free energy landscape of CORR to highlight the methanol and methane formation over HfP.

The surfaces of TaP, TiP and ZrP exhibit good catalytic activity for CO reduction, as shown in Figure 5 (a-c). This activity enables the generation of environmentally friendly products such as CH_2O, CH_3OH, and CH_4 at energy of 0.90 eV. During the fourth protonation, notably the transition from CHO* to CHOH*, we were able to see that TaP has the PDS (Figure 5(a)). However, PDS for TiP, on the other hand, was seen early after the second protonation step (CO*+MH* to CO*+MH*+PH*), exhibiting a distinct reaction route while exhibiting equivalent thermodynamic efficiency (Figure 5(b)). In the meantime, ZrP (Figure 5(c)) is also capable of reducing CO into distinctive products at a slightly greater energy of 1.04 eV. Furthermore, in a manner comparable to that of TiP, ZrP demonstrates the PDS after the second protonation during the formation of CO*+ MH*+PH* from CO*+MH*.

 doi:10.20944/preprints202603.1119.v1

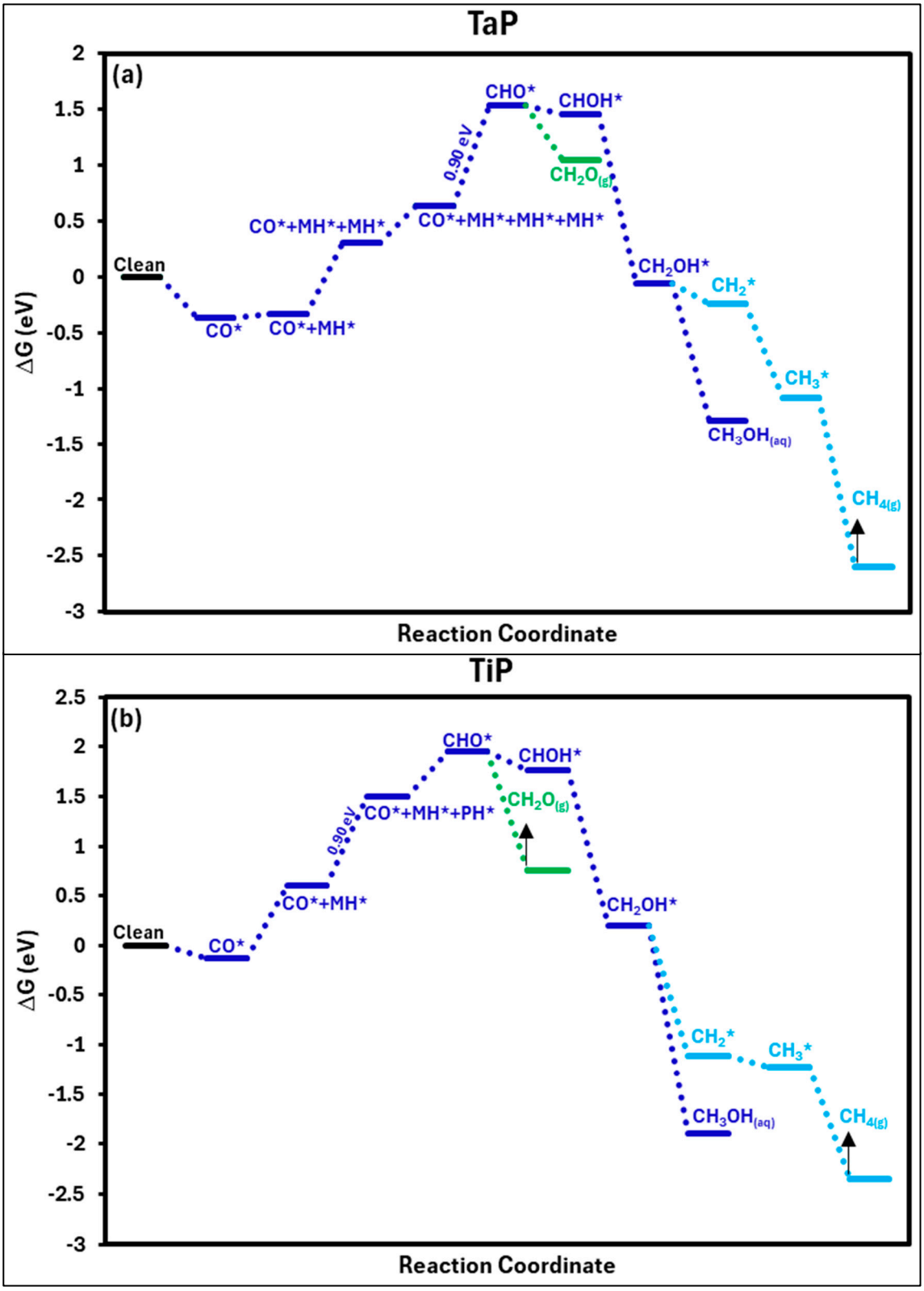

 doi:10.20944/preprints202603.1119.v1

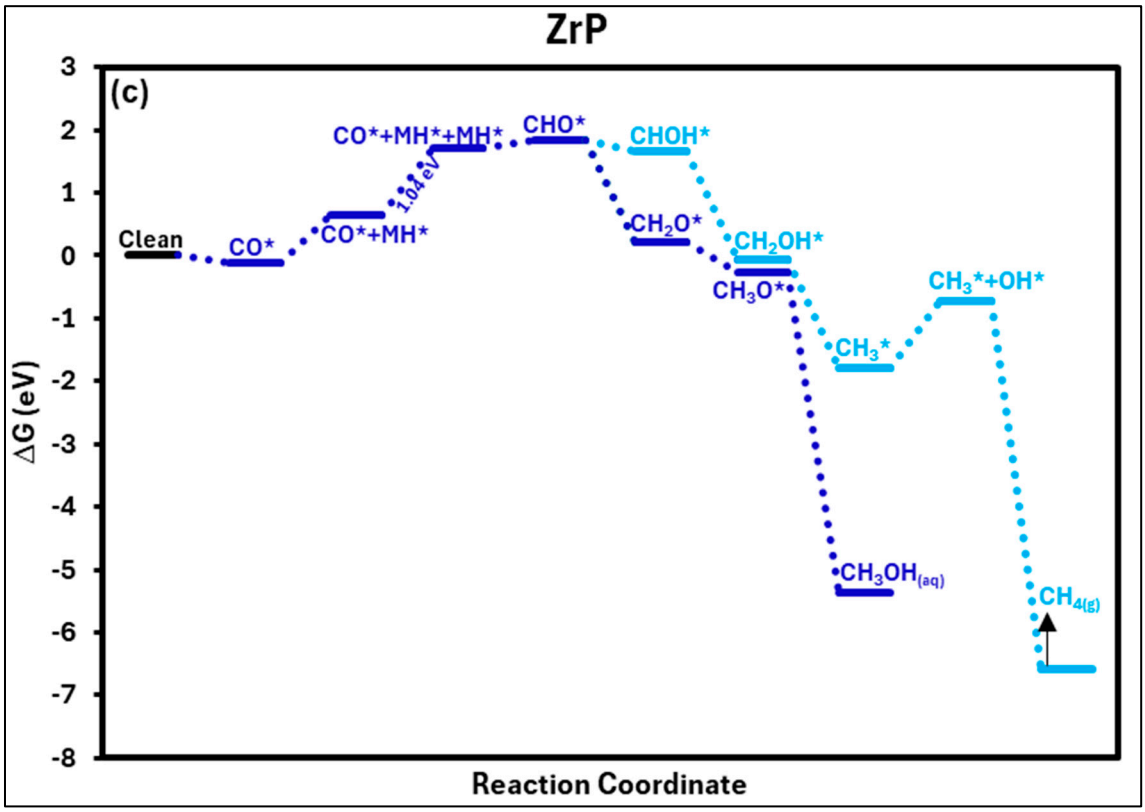

Figure 5. CO reduction pathways for formaldehyde, methanol, and methane formation over (a) TaP, (b) TiP and (c) ZrP.

3.3. Onset Potentials

To provide a concise review of our findings, we have included a comparative summary of the onset potential for CO reduction in Figure 6. This visual description offers a clear image of catalytic performance across all five TMPs, even though free energy layouts have previously been described.

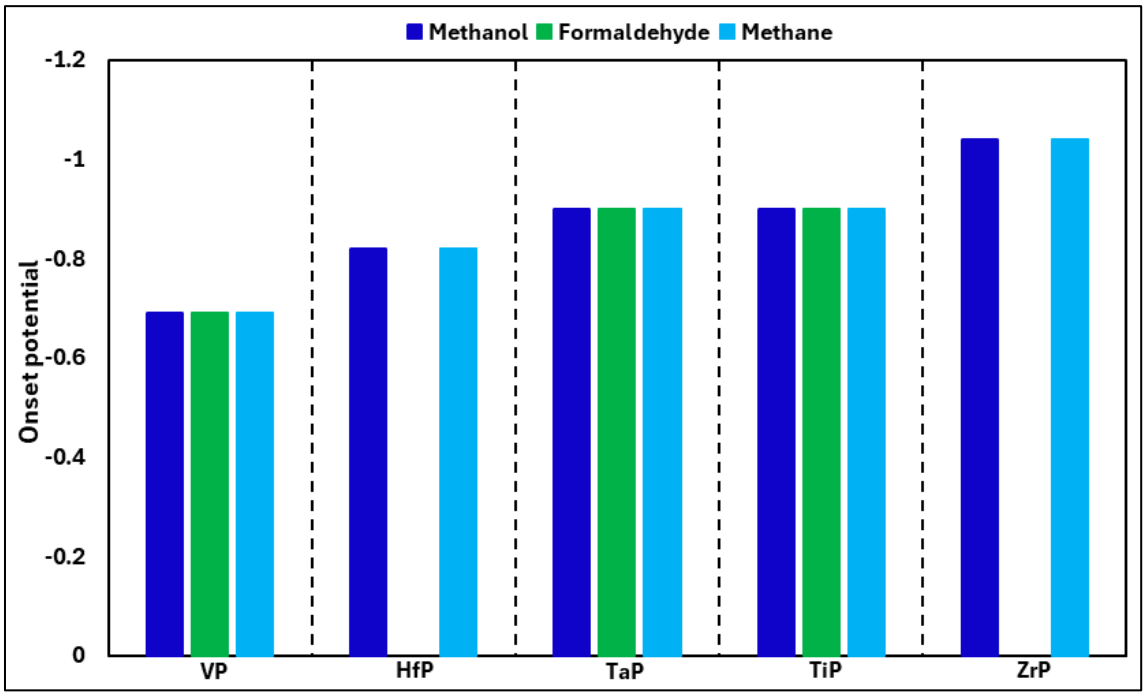

Figure 6. Comparison of onset potentials for methane, methanol and formaldehyde formation over selected TMP surfaces.

 doi:10.20944/preprints202603.1119.v1

4. Conclusions

This work used DFT to examine several surfaces composed of transition metals, such as TMPs, for the reduction of CO by electrocatalysis. We concentrated on the rock salt structures of TMPs in the (100) orientation. During the surface investigation, we noted that no surface was in the danger zone of water piousness, since each slab exhibited high CO adsorption compared to water molecules. Secondly, HER was not a concern for any surface, owing to the advantageous adsorption of CO on each TMPs. VP is designated the most active surface for CO reduction at a minimum potential of -0.69 V. VP facilitates the conversion of methane, methanol, and formaldehyde at this adjustable potential. This work presents distinct chemical pathways and a method to mitigate carbon footprints.

Acknowledgments: The calculations are carried out using the Icelandic high-performance computer cluster, Elja. Computer resources and research IT are provided by UTS of the University of Iceland through the Icelandic research e-Infrastructure project (IREI), funded by the Icelandic Infrastructure Fund. This work is supported by "The Icelandic Research Fund (RANNIS)" project grant numbers 239830–051, 239830–052, and 239830–053, and partially supported by "The Research Fund of the University of Iceland".

Conflicts of Interest: The authors declare that they have no known competing financial interests or personal relationships that could have appeared to influence the work reported in this paper.

References

1. Yoro, K.O. and M.O. Daramola, 2020, CO_2 emission sources, greenhouse gases, and the global warming effect. Advances in Carbon Capture, Elsevier: 3-28.
2. Arutyunov, V.S. and G.V. Lisichkin, 2017, Energy resources of the 21st century: problems and forecasts. Can renewable energy sources replace fossil fuels. Russian Chemical Reviews 86:777.
3. Council, N.R., et al., 2015, Climate intervention: carbon dioxide removal and reliable sequestration. National Academies Press.
4. Lee, M.-Y., et al., 2020, Current achievements and the future direction of electrochemical CO_2 reduction: A short review. Critical Reviews in Environmental Science and Technology 50:769-815.
5. Awais, M. and Y. Abghoui, 2024, Incorporating perovskites in photovoltaic-powered electrochemical cells for a sustainable future: An inclusive review. Solar Energy 282:112965.
6. Lai, W., et al., 2022, Design strategies for markedly enhancing energy efficiency in the electrocatalytic CO_2 reduction reaction. Energy & Environmental Science 15:3603-3629.
7. Wang, G., et al., 2021, Electrocatalysis for CO_2 conversion: from fundamentals to value-added products. Chemical Society Reviews 50:4993-5061.
8. Bertheussen, E., et al., 2018, Electroreduction of CO on polycrystalline copper at low overpotentials. ACS Energy Letters 3:634-640.
9. Bertheussen, E., et al., 2017, Quantification of liquid products from the electroreduction of CO_2 and CO using static headspace-gas chromatography and nuclear magnetic resonance spectroscopy. Catalysis Today 288:54-62.
10. Hao, J. and W. Shi, 2018, Transition metal (Mo, Fe, Co, and Ni)-based catalysts for electrochemical CO_2 reduction. Chinese Journal of Catalysis 39:1157-1166.
11. Fan, M., et al., 2017, Selective electroreduction of CO_2 to formate on 3D [100] Pb dendrites with nanometer-sized needle-like tips. Journal of Materials Chemistry A 5:20747-20756.
12. She, X., et al., 2022, Challenges and opportunities in electrocatalytic CO_2 reduction to chemicals and fuels. Angewandte Chemie International Edition 61:e202211396.
13. Hussain, J., H. Jónsson, and E. Skúlason, 2018, Calculations of product selectivity in electrochemical CO_2 reduction. ACS Catalysis 8:5240-5249.
14. Costentin, C., M. Robert, and J.-M. Savéant, 2013, Catalysis of the electrochemical reduction of carbon dioxide. Chemical Society Reviews 42:2423-2436.
15. Zheng, G., S. Gong, Z. Tian, H. Wang, and Q. Zhang, 2022, Theoretical screening of transition metal doped defective MoS_2 as efficient electrocatalyst for CO conversion to CH_4. ChemPhysChem 23:e202100753.

 doi:10.20944/preprints202603.1119.v1

16. Wang, W., Y. Gao, H. Li, F. Tian, D. Li, and T. Cui, 2021, Unraveling electrochemical CO reduction of the single-atom transition metals supported on N-doped phosphorene. Applied Surface Science 545:148953.
17. Chong, X., M. Hu, P. Wu, Q. Shan, Y.H. Jiang, and J. Feng, 2019, Tailoring the anisotropic mechanical properties of hexagonal M_7X_3 (M = Fe, Cr, W, Mo; X = C, B) by multialloying. Acta Materialia 169:193-208.
18. Awais, M., N. Ashraf, and Y. Abghoui, 2025, Engineering innovative catalysts for efficient CO_2 reduction toward carbon neutrality. Journal of Environmental Chemical Engineering:116621.
19. Maeda, K., A. Niitsu, H. Morito, K. Shiga, and K. Fujiwara, 2018, In situ observation of grain boundary groove at the crystal/melt interface in Cu. Scripta Materialia 146:169-172.
20. Martínez, E., U. Wiklund, J. Esteve, F. Montala, and L.L. Carreras, 2002, Tribological performance of TiN supported molybdenum and tantalum carbide coatings in abrasion and sliding contact. Wear 253:1182-1187.
21. Esteve, J., E. Martínez, A. Lousa, F. Montalá, and L.L. Carreras, 2000, Microtribological characterization of group V and VI metal-carbide wear-resistant coatings effective in the metal casting industry. Surface and Coatings Technology 133:314-318.
22. Zhang, S., 1997, Material development of titanium carbonitride-based cermets for machining application. Key Engineering Materials 138:521-544.
23. Santhanam, A.T., 1996, Application of transition metal carbides and nitrides in industrial tools. In The Chemistry of Transition Metal Carbides and Nitrides, Springer Netherlands:28-52.
24. Musil, J., 2015, Flexible hard nanocomposite coatings. RSC Advances 5:60482-60495.
25. Choe, H.J., S.H. Kwon, and J.J. Lee, 2013, Tribological properties and thermal stability of TiAlCN coatings deposited by ICP-assisted sputtering. Surface and Coatings Technology 228:282-285.
26. Seo, H.S., T.Y. Lee, J.G. Wen, I. Petrov, J.E. Greene, and D. Gall, 2004, Growth and physical properties of epitaxial HfN layers on MgO (001). Journal of Applied Physics 96:878-884.
27. Koseki, S., K. Inoue, S. Morito, T. Ohba, and H. Usuki, 2015, Comparison of TiN-coated tools using CVD and PVD processes during continuous cutting of Ni-based superalloys. Surface and Coatings Technology 283:353-363.
28. Yasuoka, M., P. Wang, and R.I. Murakami, 2012, Comparison of the mechanical performance of cutting tools coated by either a $TiCxN_{1-x}$ single-layer or a $TiC/TiC_{0.5}N_{0.5}/TiN$ multilayer using the hollow cathode discharge ion plating method. Surface and Coatings Technology 206:2168-2172.
29. Vera, E.E., M. Vite, R. Lewis, E.A. Gallardo, and J.R. Laguna-Camacho, 2011, A study of the wear performance of TiN, CrN and WC/C coatings on different steel substrates. Wear 271:2116-2124.
30. Tian, J., et al., 2014, Self-supported nanoporous cobalt phosphide nanowire arrays: an efficient 3D hydrogen-evolving cathode over the wide range of pH 0–14. Journal of the American Chemical Society 136:7587-7590.
31. Xiao, P., W. Chen, and X. Wang, 2015, A review of phosphide-based materials for electrocatalytic hydrogen evolution. Advanced Energy Materials 5:1500985.
32. Kucernak, A.R. and V.N.N. Sundaram, 2014, Nickel phosphide: the effect of phosphorus content on hydrogen evolution activity and corrosion resistance in acidic medium. Journal of Materials Chemistry A 2:17435-17445.
33. Li, X., et al., 2022, Recent advances in transition-metal phosphide electrocatalysts: Synthetic approach, improvement strategies and environmental applications. Coordination Chemistry Reviews 473:214811.
34. Kresse, G. and J. Furthmüller, 1996, Efficiency of ab-initio total energy calculations for metals and semiconductors using a plane-wave basis set. Computational Materials Science 6:15-50.
35. Hammer, B., L.B. Hansen, and J.K. Nørskov, 1999, Improved adsorption energetics within density-functional theory using revised Perdew-Burke-Ernzerhof functionals. Physical Review B 59:7413.
36. Jovanov, Z.P., et al., 2016, Opportunities and challenges in the electrocatalysis of CO_2 and CO reduction using bifunctional surfaces: A theoretical and experimental study of Au–Cd alloys. Journal of Catalysis 343:215-231.
37. Zhang, X., et al., 2023, Phosphoric acid resistance PtCu/C oxygen reduction reaction electrocatalyst for HT-PEMFCs: A theoretical and experimental study. Applied Surface Science 619:156663.

 doi:10.20944/preprints202603.1119.v1

38. Wang, H., et al., 2017, Steam methane reforming on a Ni-based bimetallic catalyst: density functional theory and experimental studies of the catalytic consequence of surface alloying of Ni with Ag. Catalysis Science & Technology 7:1713-1725.
39. Blöchl, P.E., 1994, Projector augmented-wave method. Physical Review B 50:17953.
40. Rossmeisl, J., et al., 2007, Electrolysis of water on oxide surfaces. Journal of Electroanalytical Chemistry 607:83-89.
41. Siahrostami, S. and A. Vojvodic, 2015, Influence of adsorbed water on the oxygen evolution reaction on oxides. The Journal of Physical Chemistry C 119:1032-1037.
42. Abghoui, Y., A. Iqbal, and E. Skúlason, 2023, The role of overlayered nitride electro-materials for N_2 reduction to ammonia. Frontiers in Catalysis 2:1096824.
43. Iqbal, A., E. Skúlason, and Y. Abghoui, 2024, Catalytic nitrogen reduction on the transition metal carbonitride (110) facet: DFT predictions and mechanistic insights. The Journal of Physical Chemistry C.
44. Iqbal, A., E. Skúlason, and Y. Abghoui, 2024, Are (100) facets of transition metal carbonitrides suitable as electrocatalysts for nitrogen reduction to ammonia at ambient conditions? International Journal of Hydrogen Energy 64:744-753.
45. Abghoui, Y., 2022, Superiority of the (100) over the (111) facets of the nitrides for hydrogen evolution reaction. Topics in Catalysis 65:262-269.
46. Iqbal, A., E. Skúlason, and Y. Abghoui, 2024, Electrochemical nitrogen reduction to ammonia at ambient condition on the (111) facets of transition metal carbonitrides. ChemPhysChem:e202300991.
47. Ellingsson, V., et al., 2023, Nitrogen reduction reaction to ammonia on transition metal carbide catalysts. ChemSusChem 16:e202300947.
48. Li, G., et al., 2015, Role of dissociation of phenol in its selective hydrogenation on Pt (111) and Pd (111). ACS Catalysis 5:2009-2016.
49. Nørskov, J.K., et al., 2004, Origin of the overpotential for oxygen reduction at a fuel-cell cathode. The Journal of Physical Chemistry B 108:17886-17892.
50. Xing, G., et al., 2020, Theoretical study of two-dimensional bis (iminothiolato) metal monolayers as promising electrocatalysts for carbon dioxide reduction. New Journal of Chemistry 44:12299-12306.
51. Liu, J.-H., L.-M. Yang, and E. Ganz, 2019, Electrocatalytic reduction of CO_2 by two-dimensional transition metal porphyrin sheets. Journal of Materials Chemistry A 7:11944-11952.
52. Ashraf, N., A. Iqbal, and Y. Abghoui, 2024, Exploring reaction mechanisms for CO_2 reduction on carbides. Journal of Materials Chemistry A 12:30340-30350.